Nd and Pb isotope signatures of the clay-size fraction of Labrador Sea sediments during the Holocene: Implications for the inception of the modern deep circulation pattern

N. Fagel,[1] C. Hillaire-Marcel,[2] M. Humblet,[1] R. Brasseur,[1] D. Weis,[3] and R. Stevenson[2]

Received 27 November 2003; revised 3 May 2004; accepted 12 May 2004; published 7 July 2004.

[1] Nd and Pb isotopes were measured on the fine fraction of one sediment core drilled off southern Greenland. This work aims to reconstruct the evolution of deep circulation patterns in the North Atlantic during the Holocene on the basis of sediment supply variations. For the last 12 kyr, three sources have contributed to the sediment mixture: the North American Shield, the Pan-African and Variscan crusts, and the Mid-Atlantic Ridge. Clay isotope signatures indicate two mixtures of sediment sources. The first mixture (12.2–6.5 ka) is composed of material derived from the North American shield and from a "young" crustal source. From 6.5 ka onward the mixture is characterized by a young crustal component and by a volcanic component characteristic of the Mid-Atlantic Ridge. Since the significant decrease in proximal deglacial supplies, the evolution of the relative contributions of the sediment sources suggests major changes in the relative contributions of the deep water masses carried by the Western Boundary Undercurrent over the past 8.4 kyr. The progressive intensification of the Western Boundary Undercurrent was initially associated mainly with the transport of the Northeast Atlantic Deep Water mass until 6.5 ka and with the Denmark Strait Overflow Water thereafter. The establishment of the modern circulation at 3 ka suggests a reduced influence of the Denmark Strait Overflow Water, synchronous with the full appearance of the Labrador Seawater mass. Our isotopic data set emphasizes several changes in the relative contribution of the two major components of North Atlantic Deep Water throughout the Holocene. *INDEX TERMS:* 4267 Oceanography: General: Paleoceanography; 4558 Oceanography: Physical: Sediment transport; 1040 Geochemistry: Isotopic composition/chemistry; 9325 Information Related to Geographic Region: Atlantic Ocean; 9604 Information Related to Geologic Time: Cenozoic; *KEYWORDS:* clay-size fraction, sedimentary mixings, deep circulation, Nd and Pb isotopes, North Atlantic, Labrador Sea

Citation: Fagel, N., C. Hillaire-Marcel, M. Humblet, R. Brasseur, D. Weis, and R. Stevenson (2004), Nd and Pb isotope signatures of the clay-size fraction of Labrador Sea sediments during the Holocene: Implications for the inception of the modern deep circulation pattern, *Paleoceanography*, *19*, PA3002, doi:10.1029/2003PA000993.

1. Introduction

[2] The Labrador Sea is a key site for understanding the formation of the North Atlantic Deep Water (NADW) that is largely responsible for controlling the interhemispheric heat exchange by ventilation of the world's ocean [*Broecker and Denton*, 1989]. At present, the Western Boundary Undercurrent (WBUC) is the main driving force of deep circulation in the Labrador Sea [e.g., *McCartney*, 1992]. This contour-following current drives the components of the North Atlantic Deep Water masses, mainly the Northeast Atlantic Deep Water (NEADW), the Denmark Strait Overflow Water (DSOW) and the Davis Strait Overflow (DSO) in a counter-clockwise gyre from the southern tip of Greenland to the outlet of the Labrabor Sea (Figure 1). Quaternary changes in deep oceanic circulation in the North Atlantic have been the subject of many studies [e.g., *Boyle*, 1995; *Ledbetter and Balsam*, 1985; *McCartney*, 1992; *Hillaire-Marcel et al.*, 1994; *McCave et al.*, 1995]. Sedimentological, paleontological, and/or isotopic proxies have been used to detect the presence or absence of the given components of NADW or to follow their relative production through time (Figure 2). Apart from micropaleontological assemblages, the grain size and mineralogical and isotopic composition of sediments are only indirect tracers of the water masses because they are sensitive to the particles carried by the water masses. According to grain-size data, the WBUC has been a persistent feature of the North American Continental Lower Rise during the last 30 kyr [*Ledbetter and Balsam*, 1985] and intensified at 15–16 ka [*McCave et al.*, 1995]. Foraminifera assemblages and their stable oxygen and carbon isotope compositions implicate the inception of NEADW at 9.5 ka and suggest the presence of the Northwest Atlantic Bottom Water (NWABW) (i.e., NWABW is partly (~50%) composed of DSOW) at 5.7 ka in the deep Labrador Sea [*Bilodeau et al.*, 1994]. Similarly, Nd isotopic signatures of the sediment clay-size fraction do not show any contribution of DSOW off Greenland before 8.5 ka [*Fagel et al.*, 2002]. The DSOW was thus initiated around

[1]Research Unit Clay and Paleoclimate and Mare, Department of Geology and Oceanography, University of Liège, Liège, Belgium.
[2]Centre de Recherches en Géochimie et Géodynamique (GEOTOP), Université du Québec à Montréal, Montréal, Québec, Canada.
[3]Pacific Center for Isotopic and Geochemical Research, University of British Columbia, Vancouver, British Columbia, Canada.

0883-8305/04/2003PA000993

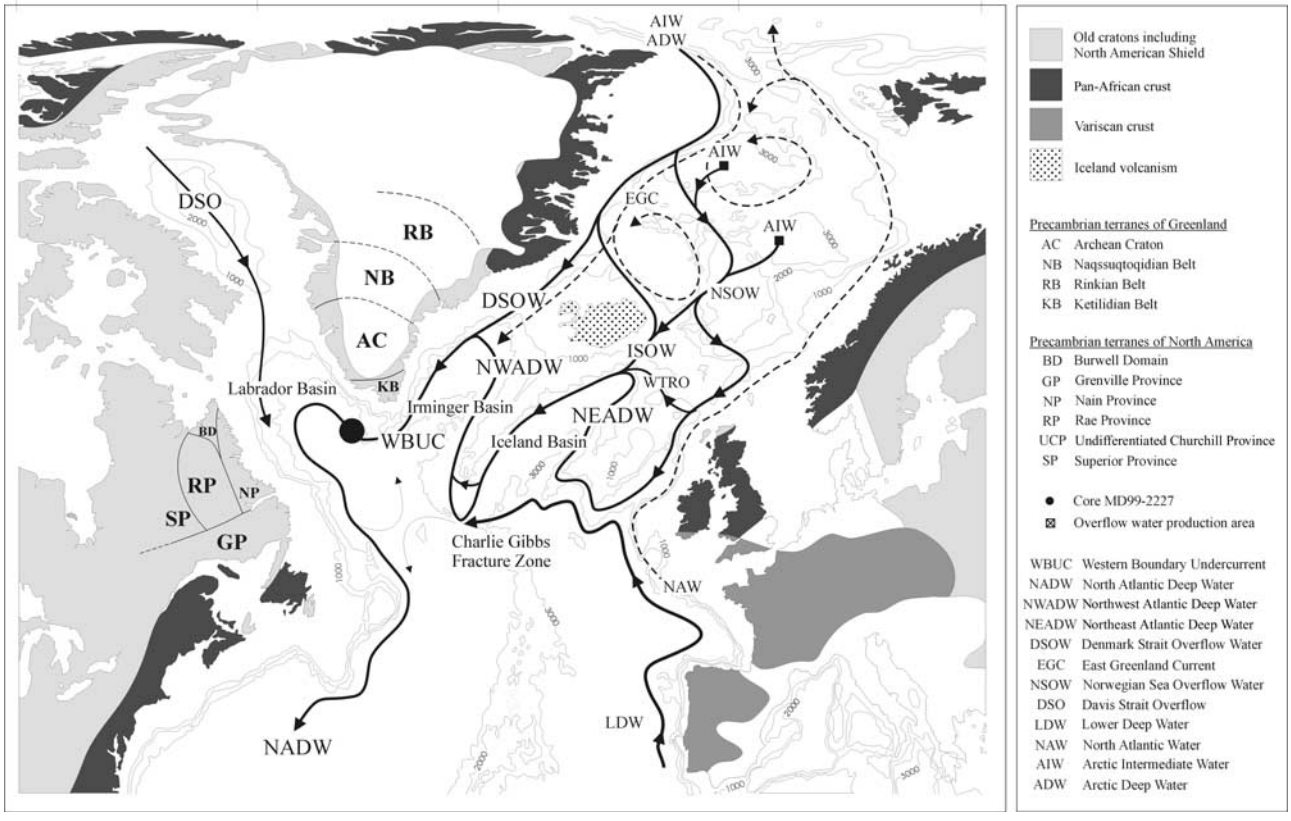

Figure 1. Location of core MD99-2227 in the Labrador Sea, northern North Atlantic. The plain arrows indicate the pathways of deep or intermediate currents modified from *McCartney* [1992], *Schmitz and McCartney* [1993], *Dickinson and Brown* [1994], *Lucotte and Hillaire-Marcel* [1994], and *Hansen and Osterhus* [2000]. The dashed arrows indicate surface circulation adapted from *Hansen and Osterhus* [2000]. The structural terranes of the continental crusts adjacent to the northern North Atlantic (data from *Bridgewater et al.* [1991], *Kalsbeek et al.* [1993], and *Campbell et al.* [1996]) are indicated by different gradations of shading (North American and Greenland Shield, Pan-African, and Variscan crusts) and by dots for mantle-derived material (Iceland volcanism).

6–8 kyr BP as indicated by ^{230}Th-excess data [*Veiga-Pires and Hillaire-Marcel*, 1998]. On the basis of micropaleontological and stable isotope data, *Hillaire-Marcel et al.* [2001a, 2001b] and *Solignac et al.* [2004] suggest that the onset of the modern thermohaline circulation occurred in three stages with a switch from the NE to the NW Atlantic routes for deep and intermediate North Atlantic Water production. During the early Holocene, maximum inflow of North Atlantic Water into the Arctic occurred [*Hillaire-Marcel et al.*, 2004; *Duplessy et al.*, 2001]. It was accompanied by a maximum production of Norwegian Sea Overflow Water (NSOW). The middle Holocene was characterized by maximum production of DSOW, whereas the late Holocene period showed maximum relative production of intermediate Labrador Seawater (LSW). Thus the present deep and intermediate circulation conditions seem to have been set up only some 4 kyr BP ago [see also *de Vernal et al.*, 2000].

[3] The aim of this paper is to further demarcate this inception of the present-day deep circulation pattern, mainly by documenting changes in the relative production rate of its DSOW component. On the basis of Nd and Pb isotope signatures of the clay-size fraction from core MD99-2227 off south Greenland, we intend to reconstruct the Holocene evolution of sedimentary supplies into the Labrador Sea that accompanied this water mass.

2. Previous Isotopic Studies

[4] Sm-Nd concentrations and Nd and Pb isotopes have been measured in the clay-size fraction of late glacial and Holocene deep-sea sediments from Labrador Sea piston core PC13 (i.e., HU90-013-013: 58°12.5N, 48°21.6W at 3379 m) raised from the vicinity of core MD99-2227. Nd and Pb isotopes in the clay-size fraction of deep sediments record how the sources of sediments and their current carriers have changed [e.g., *Dia et al.*, 1992; *Revell et al.*, 1996; *von Blanckenburg and Nägler*, 2001; *Frank*, 2002]. Nd and Pb isotope compositions record the signature of the particles supplied by the current. They can thus be used as powerful but indirect tracers of deep water circulation. In Labrador Sea sediments, Nd and Pb isotope signatures of

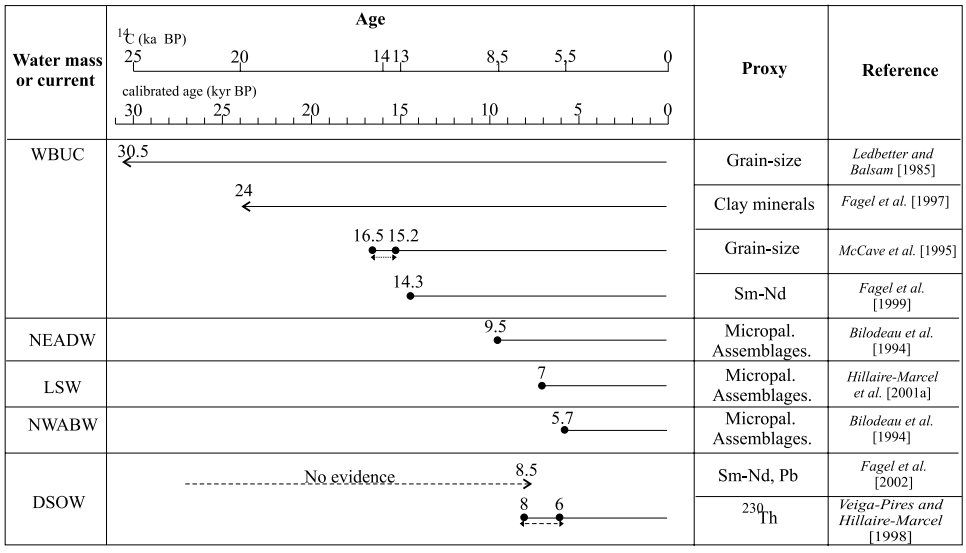

Figure 2. Historical background on the occurrence and emplacement of intermediate and deep currents in the Labrador Sea inferred from different sedimentary proxies, i.e., grain size, clay mineralogy, micropaleontological assemblages, or radiogenic (Nd, Pb, or ^{230}Th) isotopes.

late Pleistocene sediments have been interpreted to reflect mixtures of two major sources: (1) the Precambrian shield of North America and Greenland and (2) Phanerozoic upper crustal material [*Fagel et al.*, 2002]. The main contribution to deglacial sedimentary inputs off Greenland up until 8.6 kyr BP has been attributed to the Pan-African crust of northwestern Europe as a result of intensified NEADW production. Whereas modern surface sediments of this basin record major detrital contributions from the Pan-African crust of northeastern Greenland (driven by the DSOW; *Innocent et al.* [1997] and unpublished Pb data), there has been no isotopic indication of any significant input from this source prior to 8.6 ka [*Fagel et al.*, 2002].

[5] Therefore the questions that remain to be answered are: When did the Nd and Pb isotope signatures shift toward surface values? How the relative contributions of the European and Greenland Pan-African crusts evolved, relative to each other, through time? A better understanding of the evolution of sedimentary supplies and of their mixing could help to reconstruct the dynamics of the deep currents driving particles into the deep Labrador Sea during the Holocene. This, in turn, may help to better define preglobal warming oscillations and lead to a better understanding of the forcing mechanisms that drive deep-sea circulation.

3. Material

[6] Holocene sediments were sampled from Labrador Sea core MD99-2227 [*Turon et al.*, 1999]. This core was raised from the southwest Greenland Rise (58°12.64N, 48°22.38W) at a water depth of 3460 m, just below the high velocity axis of the modern WBUC (Figure 1). The total core length is 42.96 m, but this study focuses on the upper 5 m of the sediment section. This covers an interval spanning the Holocene and part of the late deglacial period, i.e., from 12.2 to 0.8 kyr BP (Figure 3). The chronology was established through linear interpolation between AMS ^{14}C ages on monospecific samples of *Neogloboquadrina pachyderma* (left coiled) assemblages, converted into calendar years using the radiocarbon calibration program Calib 4.3 (http://depts.washington.edu/qil/dloadcalib/; *Stuiver and Reimer*, 1993]) and assuming a standard marine reservoir correction of −400 years throughout the whole period. All ages reported henceforth are calibrated as kiloyears BP. The dominant lithologies of the upper 5 m of core MD99-2227 are gray nannofossil and foraminifer-rich clayey silts, nannofossil and foraminifer oozes, and burrowed clays with biogenic silica skeletons (Figure 3).

[7] The core was subsampled with a 10 cm resolution, which represents a variable time resolution due to variable sedimentation rates: ∼150 years for the 250–450 cm interval, ∼250 years for the 50–250 cm interval, ∼300 years between 0 and 50 cm, and up to 380 years for the bottom part of the sequence (from 450 to 550 cm). A total of 50 samples was analyzed for bulk sediment and clay fraction mineralogy, for grain-size determinations (through laser counting), and for Nd and Pb isotope compositions of the clay-size fraction [*Brasseur*, 2002; *Humblet*, 2002].

4. Methods

4.1. Mineralogical Analyses

[8] Mineralogical compositions were identified by X-ray diffraction (XRD) using a Bruker D8-Advance diffractometer with CuKα radiation (ULg, Belgium). For bulk mineralogy, sample powders were obtained by grinding ∼1 g of

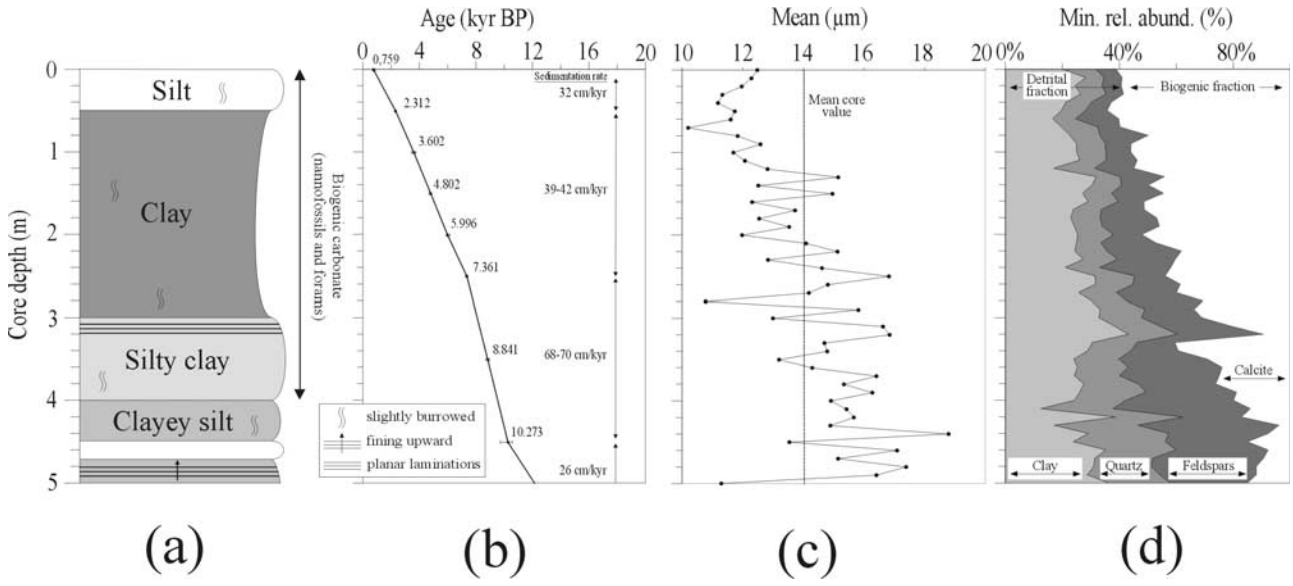

Figure 3. Core MD99-2227 description. (a) Simplified lithological column modified from *Turon et al.* [1999]. (b) Age model based on AMS^{14}C dates converted to calibrated ages using CALIB 4.3 program [*Stuiver and Reimer*, 1993] and assuming a marine reservoir correction of −400 years. The reported calibrated ages are the mean values calculated according to the method of intercepts at the 2σ level. The error bars represent the minimum and maximum calibrated age ranges around the mean value. (c) Mean grain-size value of the carbonate-free <63 μm fraction. (d) Evolution of the relative contribution of clay minerals, quartz, feldspars, and calcite in the bulk sediment deduced from X-ray diffraction measurements on powder (data from Table 2).

dried <106 μm fraction in a mortar, and a powder mount was made using the back-side method [*Moore and Reynolds*, 1989]. Semiquantitative estimates of mineralogical composition (Table 1) were obtained by applying correction factors to the measured intensity of the reflections.

[9] For clay minerals, oriented aggregates on glass slides [*Moore and Reynolds*, 1989] were prepared from the less than 2 μm fraction obtained by suspension in distilled water of ∼5 g of dried <106 μm fraction. After wet sieving, the <63 μm fraction was decarbonated in 0.1N HCl. Repeated washing and centrifugation removed the excess acid. The <2 μm was removed after a settling time estimated on the basis of Stoke's law. The operation was repeated ∼10 times in order to extract enough clay-size sediment for the isotope preparation. The first uptake was used for clay mineral analyses. Routine XRD clay analyses include the successive measurement of a X-ray pattern in air-dried condition (N), after solvatation with ethylene-glycol for 24 hours (EG), and after heating to 500°C for 4 hours (H). Semiquantitative analysis of the main clay species was based on the height of specific reflections corrected by a weight factor (Table 1).

4.2. Grain-Size Analyses

[10] Grain-size data were obtained from the <63 μm carbonate-free fraction (Table 1). The particle size distribution was determined by using a Malvern Mastersizer 2000, which measures materials from 0.02 to 2000 μm (low angle laser light scattering; ULg, Belgium). The biogenic carbonate was removed after leaching the samples with 0.1N HCl. Grain-size measurements based on the Fraunhofer and Mie theory were carried out on ∼1 g of well-dispersed homogenous sediments in liquid solution.

4.3. Nd Isotope Analyses

[11] Sm-Nd concentrations and Nd isotopic compositions were analyzed on the carbonate-free clay size fraction (<2 μm). Approximately 25 mg of ^{149}Sm/^{150}Nd spike were added to 30 mg of clay-size fraction in order to measure Sm and Nd concentrations. We followed the analytical procedure outlined in the work of *Innocent et al.* [1997]. Sm, Nd concentrations, and isotope compositions were measured on a VG Sector 54 mass spectrometer (GEOTOP, Montreal). In the course of this study, six AMES Nd standard yielded an average value of ^{143}Nd/^{144}Nd = 0.512139 ± 13 (2σ), and the LaJolla Nd standard gave an average value of 0.511849 ± 12 (n = 21) for the year that included this study. Total blanks ranged from 43 to 257 pg for both Nd and Sm and were considered negligible in comparison to the quantity of Nd (450–960 ng equivalent to 0.005–0.05%) or Sm in the sample (90–180 ng, i.e., 0.02–0.3%). Four replicates of the full analytical procedure were performed (Table 2), and they all fall within uncertainty values.

4.4. Pb Analyses

[12] For Pb isotopes, ∼20 mg of the <2 μm fraction were dissolved in a HF-HNO_3 mixture (48 hours), evaporated to dryness, redissolved in a HNO_3-HCl mixture (48 hours),

Table 1. Age and Lithological Description of Core MD99-2227: Grain Size, Bulk, and Clay Mineralogy[a]

Interval Depth, cm	Age, ^{14C} kyr BP	Error	Age Calibrated, kyr BP	Grain-Size Mean, μm	Sorting Phi	Bulk Mineralogy Clay, %	Quartz, %	Feldspar, %	Calcite, %	Clay Mineralogy I, %	Smectites, %	C, %	I-C, %	K, %	S/I
0–1	1230	±35	0.76	12.5	1.46	20	12	7	61	43	25	15	6	10	0.7
10–11			1.1	12.3	1.62	28	6	6	59	43	24	16	6	11	1.0
20–21			1.4	12.0	1.51	25	9	7	59	47	19	15	8	10	0.7
30–31			1.7	11.3	1.64	26	9	6	59	36	36	14	6	8	1.0
40–41			2.0	11.2	1.64	21	9	7	63	48	21	15	7	9	0.7
50–51	2625	±35	2.3	11.7	1.62	20	9	8	64	43	26	17	6	9	1.0
60–61			2.6	11.6	1.66	17	8	15	60	38	31	16	7	7	1.1
70–71			2.8	10.2	1.52	20	13	8	60	42	25	17	8	8	0.9
80–81			3.1	11.8	1.62	22	11	17	50	44	23	14	8	10	0.4
90–91			3.3	12.6	1.58	25	10	9	56	41	25	16	7	11	0.4
100–101	3690	±60	3.6	11.7	1.61	25	10	9	56	47	18	16	8	11	0.4
110–111			3.8	12.1	1.56	26	9	11	54	44	23	16	8	10	0.4
120–121			4.1	12.8	1.63	17	14	14	55	47	22	14	7	10	0.5
130–131			4.3	15.1	1.65	32	8	16	44	43	23	16	8	10	0.4
140–141			4.6	12.5	1.63	31	10	9	50	47	21	16	8	8	0.7
150–151	4565	±35	4.8	15.0	1.72	27	10	18	44	48	25	12	5	11	0.3
160–161			5.0	12.3	1.57	29	11	9	51	40	32	15	5	9	1.0
170–171			5.3	13.7	1.71	24	10	15	51	36	35	14	6	9	1.2
180–181			5.5	12.5	1.71	23	10	20	47	42	31	13	6	8	0.8
190–191			5.8	13.5	1.72	24	10	20	46	38	32	16	6	8	1.5
200–201	5640	±40	6.0	12.0	1.65	25	12	10	52	36	36	14	5	8	1.4
210–211			6.3	14.1	1.69	25	9	19	47	36	36	14	6	8	1.1
220–221			6.5	15.1	1.54	25	11	26	38	41	29	15	7	8	1.0
230–231			6.8	12.8	1.66	28	12	20	40	43	26	15	8	8	0.9
240–241			7.1	14.6	1.62	21	12	25	42	42	28	14	6	9	1.0
250–251	6335	±35	7.4	16.8	1.70	31	14	11	44	42	30	13	6	9	0.9
260–261			7.5	14.8	1.70	32	13	17	39	35	31	17	10	7	1.0
270–271			7.7	14.2	1.72	26	13	21	40	43	28	14	7	7	1.0
280–281			7.8	10.8	1.53	30	12	27	31	35	35	14	6	10	1.1
290–291			8.0	15.8	1.54	33	16	17	34	36	29	17	10	8	0.8
300–301			8.1	13.0	1.66	33	15	21	31	35	32	15	9	8	0.7
310–311			8.2	16.6	1.66	38	16	25	21	33	33	15	10	10	0.7
320–321			8.4	16.8	1.84	44	17	30	9	35	28	17	11	10	0.8
330–331			8.5	14.7	1.68	30	16	13	41	43	24	15	9	9	0.7
340–341			8.7	14.8	1.66	29	15	17	39	40	21	17	13	9	0.5
350–351	8300	±35	8.8	13.2	1.74	24	16	31	29	34	30	17	12	8	0.6
360–361			9.0	14.3	1.56	25	18	33	24	38	24	19	11	9	0.6
370–371			9.1	16.4	1.58	24	16	35	25	37	27	18	9	9	1.2
380–381			9.3	15.3	1.61	28	19	27	26	35	31	16	10	8	0.5
390–391			9.4	16.3	1.50	26	23	32	19	35	27	16	13	8	0.4
400–401			9.6	14.9	1.57	24	18	38	20	42	24	16	11	7	0.6
410–411			9.7	15.4	1.69	13	25	48	14	38	31	15	9	8	0.6
420–421			9.8	15.7	1.61	39	24	20	17	40	29	16	9	7	1.0
430–431			10.0	14.9	1.44	18	29	49	4	37	30	16	10	7	1.0
440–441			10.1	18.8	1.22	29	28	35	8	37	33	13	8	10	0.7
450–451	9490	±80	10.3	13.5	1.67	24	32	29	15	37	33	13	7	10	0.8
460–461			10.7	17.1	1.54	36	24	32	8	33	32	17	10	8	1.1
470–471			11.0	15.1	1.64	31	20	39	10	38	27	17	10	8	1.0
480–481			11.4	17.4	1.58	31	20	37	12	37	26	15	15	6	1.1
490–491			11.8	16.4	1.70	29	25	34	12	34	38	13	7	8	0.8
500–501			12.2	11.3	1.71	36	22	27	15	37	29	15	9	10	0.9
550–551	12510	±90													
Mean core value				14.0	1.62	27	15	21	37	40	28	15	8	8.7	0.8

[a]Data measurements were performed at a 10 cm sampling interval. For bulk mineralogy, semiquantitative estimation was obtained by applying correction factors to the measured intensity of the reflections as follows: $I_{3.34Å} \times 1$ for quartz, $I_{3.03Å} \times 1.92$ for calcite, $I_{3.18Å}$ and $I_{3.20Å} \times 2$ for feldspars, and $I_{4.4Å} \times 20$ for total clay [*Boski et al.*, 1998]. Semiquantitative estimations (±5–10%; *Biscaye* [1965]) of the main clay species were based on the height of specific reflections, generally measured on EG runs. The intensities were corrected by a weight factor and values were added up to total 100%. The relative intensity of the main clay species was calculated according to $I_{10ÅEG} \times 1$ for illite, $(I_{10ÅH}\text{-}I_{10ÅEG}) \times 1$ for smectites, $I_{14ÅEG} \times 0.4$ for chlorite, and $I_{12ÅEG} \times 0.4$ for illite-chlorite mixed layers (10–14c), $I_{7ÅEG} \times 0.7 \times [I_{3.57ÅEG}/(I_{3.57ÅEG}+I_{3.54ÅEG})]$ (see *Fagel et al.* [2003] for details). For grain-size data, mean and sorting were calculated according to *Folk and Ward* [1957].

evaporated, redissolved in HCl, again evaporated, and finally dissolved in 0.8N HBr. Pb was chemically extracted by using AG1-X8 anion columns in a HBr environment [*Manhès et al.*, 1978]. The Pb isotopes were measured in static mode using a MC-ICP-MS Nu plasma instrument (ULB, Belgium) with standard bracketing in order to take into account a potential analytical drift. The standard used was NIST981 (200 ppb Pb, to which 50 ppb Tl were added in HNO_3 0.05N environment). A thallium spike was added to all samples and standards to monitor mass fractionation

Table 2. Nd and Pb Isotopic Data From Carbonate-Free Clay Size <2 μm Material From Piston Core MD99-2227 on the Greenland Rise[a]

Interval Depth, cm	Age, kyr BP	Sm, ppm	Nd, ppm	$^{147}Sm/^{144}Nd$	$^{143}Nd/^{144}Nd$	±2σ × 10^{-6}	εNd	$^{206}Pb/^{204}Pb$	±2σ × 10^{-4}	$^{207}Pb/^{204}Pb$	±2σ × 10^{-4}	$^{208}Pb/^{204}Pb$	±2σ × 10^{-4}	$^{207}Pb/^{206}Pb$	±2σ × 10^{-4}	$^{208}Pb/^{206}Pb$	±2σ × 10^{-4}
0	0.76	6.0	29	0.12617	0.512159	15	−9.3	18.7234	11	15.6048	9	38.8507	37	0.8334	0.2	2.0749	1.8
								18.7225	**7**	**15.6024**	**6**	**38.8462**	**23**	**0.8334**	**0.3**	**2.0749**	**1.4**
10– 11	1.1	5.8	28	0.1245	0.512146	10	−9.6	18.8181	12	15.5910	10	38.9755	43	0.8285	0.2	2.0713	1.3
20–21	1.4	5.9	28	0.1270	0.512160	11	−9.3	18.8486	12	15.5989	11	39.0567	48	0.8276	0.2	2.0722	1.2
								18.8563	**6**	**15.6015**	**7**	**39.0694**	**21**	**0.8274**	**0.1**	**2.0719**	**0.8**
30–31	1.7	4.8	24	0.1231	0.512119	10	−10.1	18.8081	13	15.5921	9	39.0190	30	0.8290	0.2	2.0744	3.1
40–41	2.0	5.8	29	0.1226	0.512110	25	−10.3	18.7685	12	15.5928	11	38.9468	62	0.8308	0.2	2.0751	1.2
50–51	2.3	5.9	28	0.1263	0.512174	10	−9.1	18.8287	14	15.6026	13	39.0364	39	0.8287	0.2	2.0732	1.1
60–61	2.6	4.7	24	0.1224	0.512133	11	−9.8	18.8196	23	15.5905	21	39.0218	57	0.8284	0.2	2.0734	0.6
70–71	2.8	4.5	22	0.1212	0.512139	12	−9.7	18.8093	16	15.5921	14	38.9695	43	0.8290	0.2	2.0718	1.5
		4.5	**22**	**0.1211**	**0.512128**	**8**	**−10.0**										
80–81	3.1	2.9	15	0.1145	0.512097	8	−10.5	18.4484	50	15.5139	42	38.6978	11	0.84	0.3	2.10	0.9
90–91	3.3	3.1	16	0.1161	0.512102	14	−10.5	18.6377	21	15.5502	23	38.8889	67	0.8344	0.3	2.0866	1.4
								18.6324	**12**	**15.5520**	**10**	**38.8792**	**46**	**0.8346**	**0.2**	**2.0865**	**1.1**
100–101	3.6	3.6	18	0.1170	0.512106	9	−10.4	18.6096	0	15.5194	0	38.7505	0	0.83	0.0	2.08	0.0
110–111	3.8	3.0	16	0.1152	0.512094	10	−10.6	18.4982	24	15.5380	24	38.7276	50	0.8400	0.2	2.0937	2.5
120–121	4.1	3.4	18	0.1165	0.512097	11	−10.6	18.6296	29	15.5423	26	38.8497	71	0.8343	0.2	2.0853	0.9
130–131	4.3	3.4		0.1166	0.512122	9	−10.1	18.5852	42	15.5360	31	38.8110	82	0.8360	0.2	2.0881	1.4
		3.4	**17**	**0.1166**	**0.512115**	**13**	**−10.2**										
140–141	4.6	3.6	18	0.1172	0.512101	19	−10.5	18.6497	29	15.5545	23	38.9021	128	0.8340	0.3	2.0859	2.2
150–151	4.8	3.4	18	0.1161	0.512104	17	−10.4	18.5846	21	15.5350	17	38.8445	50	0.8359	0.2	2.0900	1.8
160–161	5.0	4.1	21	0.1190	0.512141	7	−9.7	18.7659	16	15.5734	15	39.0189	53	0.8299	0.2	2.0791	1.5
170–171	5.3							18.8596	15	15.5936	14	39.1159	43	0.8268	0.2	2.0740	1.7
								18.8648	**26**	**15.5926**	**18**	**39.1037**	**56**	**0.8266**	**0.2**	**2.0727**	**1.3**
180–181	5.5	3.9	20	0.1177	0.512117	9	−10.2	18.6389	26	15.5544	24	38.8692	64	0.8345	0.2	2.0852	0.8
190–191	5.8	4.0	21	0.1185	0.512105	8	−10.4	18.7773	23	15.5715	21	39.0393	66	0.8293	0.2	2.0789	1.1
200–201	6.0	4.3	22	0.1186	0.512099	10	−10.5	18.8372	19	15.5839	16	39.0784	61	0.8273	0.1	2.0744	0.9
210–211	6.3	4.6	23	0.1202	0.512116	7	−10.2	18.8829	20	15.5911	18	39.1501	65	0.8257	0.2	2.0732	1.2
220–221	6.5	4.1	21	0.1184	0.512078	8	−10.9	18.7234	12	15.5675	10	38.9825	41	0.8314	0.1	2.0818	0.8
230–231	6.8	4.3	22	0.1177	0.512059	9	−11.3	18.7175	9	15.5829	8	38.9609	32	0.8325	0.2	2.0815	1.6
240–241	7.1	4.2	22	0.1169	0.512052	9	−11.4	18.7586	18	15.5550	16	39.0781	46	0.8292	0.2	2.0833	0.7
250–251	7.4	4.0	21	0.1155	0.512022	9	−12.0	18.6576	23	15.5472	21	39.0230	56	0.8333	0.4	2.0915	2.8
260–261	7.5	3.9	21	0.1149	0.511997	9	−12.5	18.5477	18	15.5296	16	38.8911	41	0.8373	0.2	2.0967	0.6
270–271	7.7	4.8	25	0.1170	0.512003	9	−12.4	18.7604	9	15.5669	8	39.1476	28	0.8298	0.1	2.0866	0.9
280–281	7.8	3.9	21	0.1145	0.511963	7	−13.2	18.4751	41	15.5048	36	38.9054	93	0.8392	0.2	2.1059	0.8
290–291	8.0	3.9	20	0.1139	0.511918	9	−14.0	18.3105	32	15.4909	26	38.8242	81	0.8460	0.1	2.1200	1.1
300–301	8.1	4.0	21	0.1135	0.511875	9	−14.9	18.2851	21	15.4692	19	38.8356	52	0.8460	0.2	2.1239	0.7
310–311	8.3	3.5	19	0.1116	0.511799	30	−16.4	17.9759	37	15.4203	38	38.7238	99	0.8577	0.4	2.1541	0.9
		3.5	**19**	**0.1115**	**0.511813**	**8**	**−16.1**										
320–321	8.4	3.6	20	0.1126	0.511845	9	−15.5	18.3064	24	15.4889	20	38.8260	63	0.8461	0.2	2.1207	2.4
330–331	8.5	4.4	18		0.511983	9	−12.8										
340–341	8.7	4.0	21	0.1153	0.512016	5	−12.1	18.6155	24	15.5388	21	38.9108	60	0.8347	0.2	2.0901	0.9
350–351	8.8	5.1	29		0.512028	10	−11.9										
360–361	9.0	4.0	21	0.1145	0.511966	15	−13.1	18.6019	21	15.5241	19	38.9266	49	0.8345	0.2	2.0925	1.3
370–371	9.1	6.5	32		0.512084	10	−10.8										
380–381	9.3	4.1	22	0.1153	0.511979	8	−12.9	18.6321	31	15.5252	23	38.9647	75	0.8333	0.1	2.0910	0.9
400–401	9.6	5.3	27	0.1178	0.511965	5	−13.1	18.7738	15	15.5393	13	39.1368	34	0.8277	0.2	2.0845	1.8
410–411	9.7	4.6	24	0.1142	0.511921	9	−14.0										
420–421	9.8	5.5	29	0.1139	0.511844	6	−15.5	18.5743	16	15.4783	13	39.0808	48	0.8333	0.2	2.1041	1.1

Table 2. (continued)

Interval Depth, cm	Age, kyr BP	Sm, ppm	Nd, ppm	$^{147}Sm/^{144}Nd$	$^{143}Nd/^{144}Nd$	±2σ × 10^{-6}	εNd	$^{206}Pb/^{204}Pb$	±2σ × 10^{-4}	$^{207}Pb/^{204}Pb$	±2σ × 10^{-4}	$^{208}Pb/^{204}Pb$	±2σ × 10^{-4}	$^{207}Pb/^{206}Pb$	±2σ × 10^{-4}	$^{208}Pb/^{206}Pb$	±2σ × 10^{-4}
430–431	10.0	4.9	27	0.1089	0.511696	9	−18.4										
440–441	10.1	4.5	24	0.1113	0.511707	5	−18.2	17.7321	31	15.3265	34	38.1493	68	0.8643	0.2	2.1514	1.0
		4.4	**24**	**0.1111**	**0.511711**	**10**	**−18.1**	**17.8024**	**11**	**15.3427**	**11**	**38.2405**	**54**	**0.8618**	**0.2**	**2.1481**	**2.4**
450–451	10.3	4.4	24	0.1138	0.511866	16	−15.1	18.5923	23	15.5077	22	38.9033	61	0.8340	0.1	2.0924	1.3
460–461	10.7	3.9	21	0.1144	0.511943	7	−13.6	18.5454	32	15.4958	33	38.8598	84	0.8356	0.2	2.0952	1.8
470–471	11.0	4.6	24	0.1154	0.511934	9	−13.7	18.7170	25	15.5183	21	38.9663	57	0.8291	0.2	2.0819	1.1
480–481	11.4	4.1	22	0.1135	0.511916	13	−14.1										
490–491	11.8	4.1	23	0.1094	0.511787	9	−16.6	18.3414	23	15.4535	21	38.7978	73	0.8426	0.2	2.1151	1.2
500–501	12.2	3.6	20	0.1089	0.511771	11	−16.9	17.9772	28	15.3984	32	38.4772	93	0.8565	0.2	2.1402	1.1

[a] εNd is calculated as follows: $[(^{143}Nd/^{144}Nd_{sample}/^{143}Nd/^{144}Nd_{CHUR}) - 1] \times 10^4$, where the Nd isotopic ratio for chondritic undifferenciated reservoir (CHUR) is 0.512638 [*Wasserburg et al.*, 1981]. Boldface represents replicate analysis values.

[*White et al.*, 2000], assuming that Tl and Pb are characterized by similar mass fractionation [*Rosman and Taylor*, 1998]:

$$f_{Tl} = \ln\left(\left(^{205}Tl/^{203}Tl\right)_{measured} / \left(^{205}Tl/^{203}Tl\right)_{true}\right) / \ln\left(^{mass205}Tl/^{mass203}Tl_{true}\right),$$

where $(^{205}Tl/^{203}Tl)_{true} = 2.3885$; $^{mass205}Tl/^{mass203}Tl_{true} = 1.00986$. The mass fractionation corrected isotopic ratio was then calculated according to:

$$\left(^{208}Pb/^{204}Pb\right)_{corrected} = \left(^{208}Pb/^{204}Pb\right)_{measured} \times \left(^{mass208}Pb/^{mass204}Pb\right)^{-fTl}.$$

Because the Tl/Pb ratio appears to be critical to the accuracy of the Pb isotope results, only results for samples with Tl/Pb < 0.5 were retained.

[13] Replicates of the entire analytical procedure ($n = 5$) are reported in Table 2, and all but one (see replicate 440–441) fall within error bars. Total blank estimates ranged from 40 to 200 pg, i.e., entirely negligible in comparison to the quantity of Pb in the sample (100–500 ng). In the course of the study, 400 measurements of NBS981 yielded average values of 36.712 ± 0.011 (2σ) for $^{208}Pb/^{204}Pb$, 15.4954 ± 0.0041 for $^{207}Pb/^{204}Pb$, 16.9389 ± 0.0045 for $^{206}Pb/^{204}Pb$, 0.92478 ± 0.0009 for $^{207}Pb/^{206}Pb$, and 2.16730 ± 0.0032 for $^{208}Pb/^{206}Pb$ and are within error of the triple spike values [*Galer*, 1999].

5. Results

5.1. Sediment Characterization

5.1.1. Mineralogy

[14] The relative abundances of clay minerals, quartz, feldspars, and calcite are reported in Figure 3 (data from Table 1). In addition, amphibole (not taken into account in Figure 3) is ubiquitous in the bulk sediment and represents ~10% of the total sediment. The calcite content (mean 37%) increases gradually from 10% at 12.2 ka to a present-day value of 60%. A significant decrease in calcite is observed at 8.4 and 10 ka and counterbalanced by an increase in feldspar content. Quartz and feldspars average 15 and 21% of the bulk mineralogy, respectively. The clay mineral proportion fluctuates around an average value of 27% over the Holocene. Within the carbonate-free fraction the clays significantly increase through the Holocene (e.g., 70% at 1.1 ka).

[15] Within the < 2 μm fraction, the clay mineral assemblage is composed of 40% illite, 28% smectite, 15% chlorite, 9% kaolinite, and 8% illite-chlorite. The smectite/illite ratio (i.e., $S/I = I_{17ÅEG}/I_{10ÅEG}$) ranges from 0.35 to 1.5 (mean 0.8) through time (Table 1). It shows a sharp increase at 8.4 ka and culminated ~5.8 kyr ago, with a value of 1.5. The ratio then fell quite abruptly to a minimum value of 0.35 at 4.8 ka and remained very low until about 3 ka. The

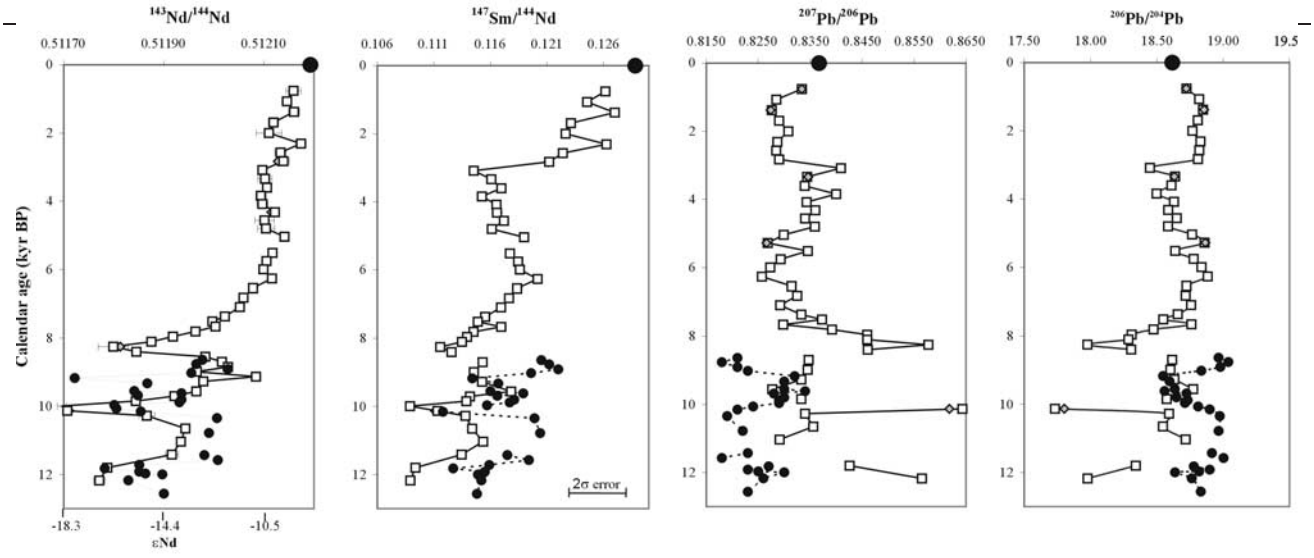

Figure 4. $^{143}Nd/^{144}Nd$, $^{147}Sm/^{144}Nd$, $^{207}Pb/^{206}Pb$, and $^{206}Pb/^{204}Pb$ ratios of the clay-size fraction of cores MD99-2227 (squares) and PC13 (circles; data from *Fagel et al.* [2002]) as a function of calibrated ages. The signature of surface sediment is also plotted (data from *Innocent et al.* [1997]). Replicates (diamonds) and analytical errors are reported (i.e.,±2 standard deviations for Nd and Pb ratios, 2% of the measured value for the Sm/Nd ratios). For Pb ratios the errors are smaller than symbol size.

smectite/illite ratio then rose suddenly to reach values that fluctuate within a range similar to that of the interval prior to the 8.4 ka shift. The lower part of the section (older than 8.4 kyr) is strongly depleted in smectite in comparison with core PC13 ($1.5 < S/I < 7$ in PC13 with a mean of 3.4). This is likely due to a site specific effect, core MD99-2227 being 80 m deeper than PC13 and hence 80 m below the main WBUC influence.

5.1.2. Grain Size

[16] In the <63 μm carbonate-free fraction the particle size distribution is unimodal. The mean grain size (according to *Folk and Ward* [1957]) ranges between 10.2 (at 2.8 kyr BP) and 18.8 μm (at 10.1 kyr BP). It fluctuates around a mean value of 14 μm but exhibits large variations within short time intervals, especially near 10.1, 8.2–8.4, and 7.4 ka (Figure 3). The mean grain size usually displays values higher than the core section mean value prior to 6 ka, and lower values since then, with a clear decrease between 3.8 and 1.4 ka. The lowest sorting was recorded at precisely 8.4 ka (Table 2).

5.2. Nd and Pb Isotopic Signatures of the Clay Fraction

[17] In MD99-2227, Nd isotopic ratios in the clay-size fraction range from 0.511696 to 0.512174 and $^{147}Sm/^{144}Nd$ ratios from 0.1089 to 0.1270 (Table 2, Figure 4). The overall trends are an increase in both $^{143}Nd/^{144}Nd$ and $^{147}Sm/^{144}Nd$ ratios over the past 12 kyr. Since 8.2 ka the Nd isotopic ratios have shifted toward higher values, reaching up to 0.512116 between 6.3 a and the present day. Prior to 8.2 ka the Nd isotopic compositions display a wide range of variations (~8 εNd). Samples younger than 6 kyr are characterized by more radiogenic and less variable Nd isotopic compositions (<1 εNd). $^{147}Sm/^{144}Nd$ ratios display a somewhat similar pattern, but the shift toward higher values (from 0.1145 to 0.1212) occurs during the last 3 kyr only.

[18] For the Pb isotopic system the ratios $^{206}Pb/^{204}Pb$, $^{207}Pb/^{204}Pb$, and $^{208}Pb/^{204}Pb$ all display similar downcore profiles. For instance, the $^{206}Pb/^{204}Pb$ ratios fluctuate between 17.73 and 18.86, with less marked variations in the younger samples (Table 2 and Figure 4).

[19] Data from core PC13 are shown for comparison with those of MD99-2227. There is a good agreement for the Nd isotopic signatures in both cores. For Pb the agreement is not as good, which may reflect the different techniques used (TIMS versus MC-ICP-MS). Our new data are about 10 times more precise. The $^{143}Nd/^{144}Nd$, $^{147}Sm/^{144}Nd$, and Pb (with only $^{207}Pb/^{206}Pb$ reported on Figure 4) ratios all converge toward the PC13 surface isotopic composition [*Innocent et al.*, 1997]. However, the $^{147}Sm/^{144}Nd$ ratios in PC13 are higher than those in core MD99-2227. The difference usually stands within analytical errors, but the trend is nonetheless systematic. It is more likely due to the different coring locations of PC 13 and MD99-2227 with respect to the main velocity axis of the WBUC than to any analytical bias between the two analysis periods. We note too that the different isotope signatures of the two cores are carried by different mineralogical assemblages (see section 5.1.1).

[20] Superimposed on the overall trends are sharp minima for $^{143}Nd/^{144}Nd$, $^{147}Sm/^{144}Nd$ ratios, and maxima for isotopic Pb ratios at 10 and 8.2 ka. The 10 ka event is the most pronounced and is also recorded in PC13.

6. Discussion

6.1. Sedimentary Provenance Inferred From Nd and Pb Signatures of the Clay-Size Fraction

6.1.1. Identification of the Geographical Source Areas

[21] The interpretation of sedimentary provenance requires knowledge of the different potential geographical

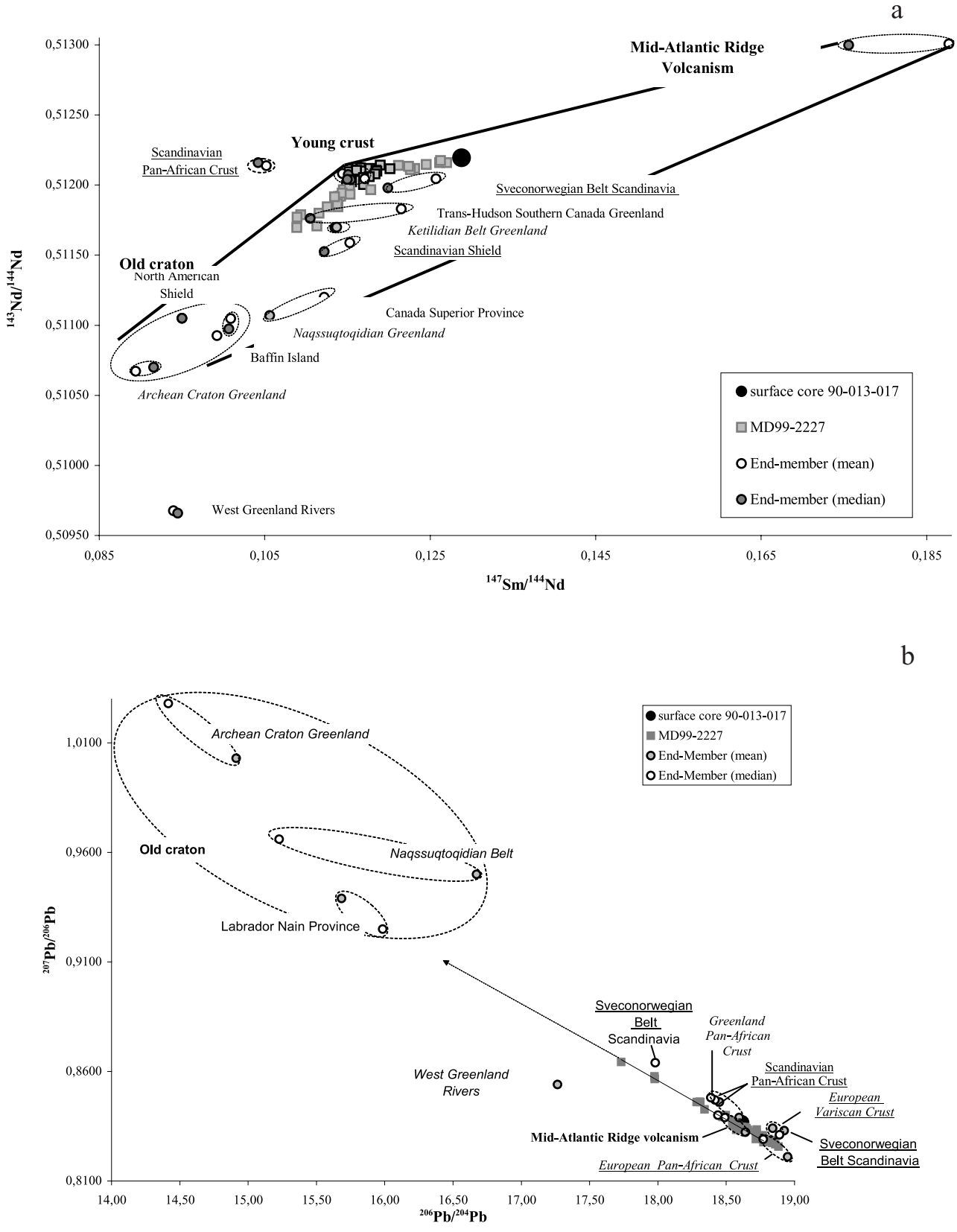
a
Mid-Atlantic Ridge Volcanism
Young crust
Scandinavian Pan-African Crust
Sveconorwegian Belt Scandinavia
Trans-Hudson Southern Canada Greenland
Ketilidian Belt Greenland
Scandinavian Shield
Old craton
North American Shield
Canada Superior Province
Naqssuqtoqidian Greenland
Baffin Island
Archean Craton Greenland
West Greenland Rivers
surface core 90-013-017
MD99-2227
End-member (mean)
End-member (median)
143Nd/144Nd
147Sm/144Nd
0,51300
0,51250
0,51200
0,51150
0,51100
0,51050
0,51000
0,50950
0,085
0,105
0,125
0,145
0,165
0,185
b
surface core 90-013-017
MD99-2227
End-Member (mean)
End-Member (median)
Archean Craton Greenland
Old craton
Naqssuqtoqidian Belt
Labrador Nain Province
Sveconorwegian Belt Scandinavia
Greenland Pan-African Crust
Scandinavian Pan-African Crust
European Variscan Crust
West Greenland Rivers
Mid-Atlantic Ridge volcanism
European Pan-African Crust
Sveconorwegian Belt Scandinavia
207Pb/206Pb
206Pb/204Pb
1,0100
0,9600
0,9100
0,8600
0,8100
14,00
14,50
15,00
15,50
16,00
16,50
17,00
17,50
18,00
18,50
19,00

Figure 5

source areas. The isotopic data for the clay-size fraction of MD99-2227 are presented in a $^{143}Nd/^{144}Nd$ versus $^{147}Sm/^{144}Nd$ diagram (Figure 5a) and a $^{207}Pb/^{206}Pb$ versus $^{206}Pb/^{204}Pb$ diagram (Figure 5b). The data are plotted with reference to potential end-members (data in the work of *Fagel et al.* [2002]). The potential regional sources are represented by their mean and median values in order to underscore the uncertainty of each end-member. The Pb-Pb isotope data of core MD99-2227 are distributed along a two end-member mixing line. The European Pan-African crust is identified as one potential end-member (named here "young crust") and is characterized by low $^{207}Pb/^{206}Pb$ and high $^{206}Pb/^{204}Pb$ ratios. The Scandinavian Sveconorwegian Belt is rejected because its $^{143}Nd/^{144}Nd$ signature is too low to account for the observed Sm-Nd data. An additional minor contribution from the European Variscan crust cannot be discarded but cannot be distinguished from other young crust candidates on the basis of Sm-Nd signatures alone. The Greenland Archean Craton, Naqssuqtoqidian Belt, or Labrador Nain Province are all good candidates for the high $^{207}Pb/^{206}Pb$ and low $^{206}Pb/^{204}Pb$ ratios end-member (named here "old craton"). Both Baffin Island and the North American Shield are characterized by Sm-Nd signatures compatible with the old craton end-member. In addition to supplies from the young crust and old craton terranes, a third mantle-like contribution characterized by high $^{147}Sm/^{144}Nd$ and $^{143}Nd/^{144}Nd$ ratios must be taken into account to explain Sm-Nd data. This component is attributed to Mid-Atlantic Ridge (MAR) volcanism.

6.1.2. Evolution of Sedimentary Provenances Through the Holocene

[22] Sm-Nd data in core MD99-2227 illustrate two distinct time-related linear trends (Figure 6a). The first one (from 12.2 to 6.5 ka) may be mainly characterized by the mixing of material derived from the old cratons and young crust, plus a minor contribution from MAR volcanism material. After 6.5 ka, isotopic signatures require a more significant contribution of MAR material instead of the old craton material; this shift toward the MAR end-member is particularly marked after 3 ka.

[23] In the Pb-Pb mixing diagram of Figure 6b, all samples younger than 6.5 ka fall between two Pan-African crustal end-members. We estimate the relative contributions of the crustal end-members by projecting data onto the mixing line between the median value for the Greenland Pan-African Crust (GPC) and the mean value for the European Pan-African Crust (EPC). Note that a contribution from the Scandinavian Pan-African Crust (SPC) cannot be definitely ruled out. Any mixing calculation between SPC and EPC whatsoever would not change the interpretation in terms of the evolution of the sedimentary sources: It will result in a systematically higher relative contribution of the EPC in the mixing estimates. The oceanographic implications will be discussed in a later section. For samples younger than 6.5 kyr BP, the influence of MAR as a third possible end-member is not obvious from the Pb-Pb mixing diagram. The low sensitivity of the Pb isotope system to any increase in MAR volcanics simply reflects the low Pb content in volcanic-derived material (~500 ppb). The influence of MAR is especially obvious in a combined Sm-Pb mixing diagram (Figure 7).

[24] Finally, four end-members have been retained for mixing calculations: (1) the North American Shield (NAS), (2) the Mid-Atlantic Ridge (MAR) volcanism, (3) the European Pan-African Crust (EPC), and (4) the Greenland Pan-African Crust (GPC). For our calculations, we first used a standard Sm-Nd mixing between three end-members, i.e., NAS, MAR, and undifferentiated YC. The three variables are the $^{147}Sm/^{144}Nd$ ratio, the $^{143}Nd/^{144}Nd$ ratio, and the Nd content of each end-member: The values are reported in Figure 6a. The Sm content is calculated from the Nd content and the chemical $^{147}Sm/^{144}Nd$ ratio. We calculate a mixing grid on the basis of different proportions of the three end-members. For each grid point we calculate the Nd and the Sm isotope signature taking into account the contribution of the three end-members (1, 2, 3) as follows [e.g., *Faure*, 1986]:

$$^{143}Nd/^{144}Nd\ \text{ratio}_{mix} = \frac{\alpha_1[Nd]_1\left(^{143}Nd/^{144}Nd\right)_1 + \alpha_2[Nd]_2\left(^{143}Nd/^{144}Nd\right)_2 + \alpha_3[Nd]_3\left(^{143}Nd/^{144}Nd\right)_3}{[Nd]_{mix}}$$

$$^{147}Sm/^{144}Nd\ \text{ratio}_{mix} = \left([Sm]_{mix}/[Nd]_{mix}\right) \times 0.60847$$

$$[Nd]mix = \alpha_1 \times [Nd]_{1+}\ \alpha_2 \times [Nd]_{2+}\ \alpha_3 \times [Nd]_3$$

$$[Sm]mix = \alpha_1 \times [Sm]_{1+}\ \alpha_2 \times [Sm]_{2+}\ \alpha_3 \times [Sm]_3$$

$$\alpha_1 + \alpha_2 + \alpha_3 = 1.$$

Second, for the YC, an estimate of the relative contribution of the European and Greenland Pan-African crusts is derived from the Pb isotope system. Note that discrimination between the two Pan-African components is only possible for samples younger than 6.5 ka, the older samples being too strongly influenced by deglacial NAS supplies (see Figure 6b).

[25] Plots of the relative contributions of the four end-members (Figure 8) may be subdivided into four time periods taking into account the NAS contribution: (1) from 12.2 to 7.8 ka, (2) 7.7 to 5.8 ka, (3) 5.5 to 3.3 ka, and (4) 3.1 ka to present.

6.1.2.1. Time Period 12.2 to 7.8 ka

[26] The sedimentary supplies display large variations, highlighted by sharp changes in the Nd and Pb isotope

Figure 5. (a) $^{147}Sm/^{144}Nd$ versus $^{143}Nd/^{144}Nd$ diagram. All data from core D99-2227 are plotted (shaded squares) with regard to the surface sediment PC13 core sample (filled circles) and the potential clay sources. The regional sources are represented by their mean and median values in order to underscore the uncertainty of each end-member, especially the old craton (data from *Fagel et al.* [2002]). (b) $^{207}Pb/^{206}Pb$ versus $^{206}Pb/^{204}Pb$ diagram for core MD99-2227 (shaded squares) and potential regional sources. The linear regression trend for all the MD99-2227 data is plotted.

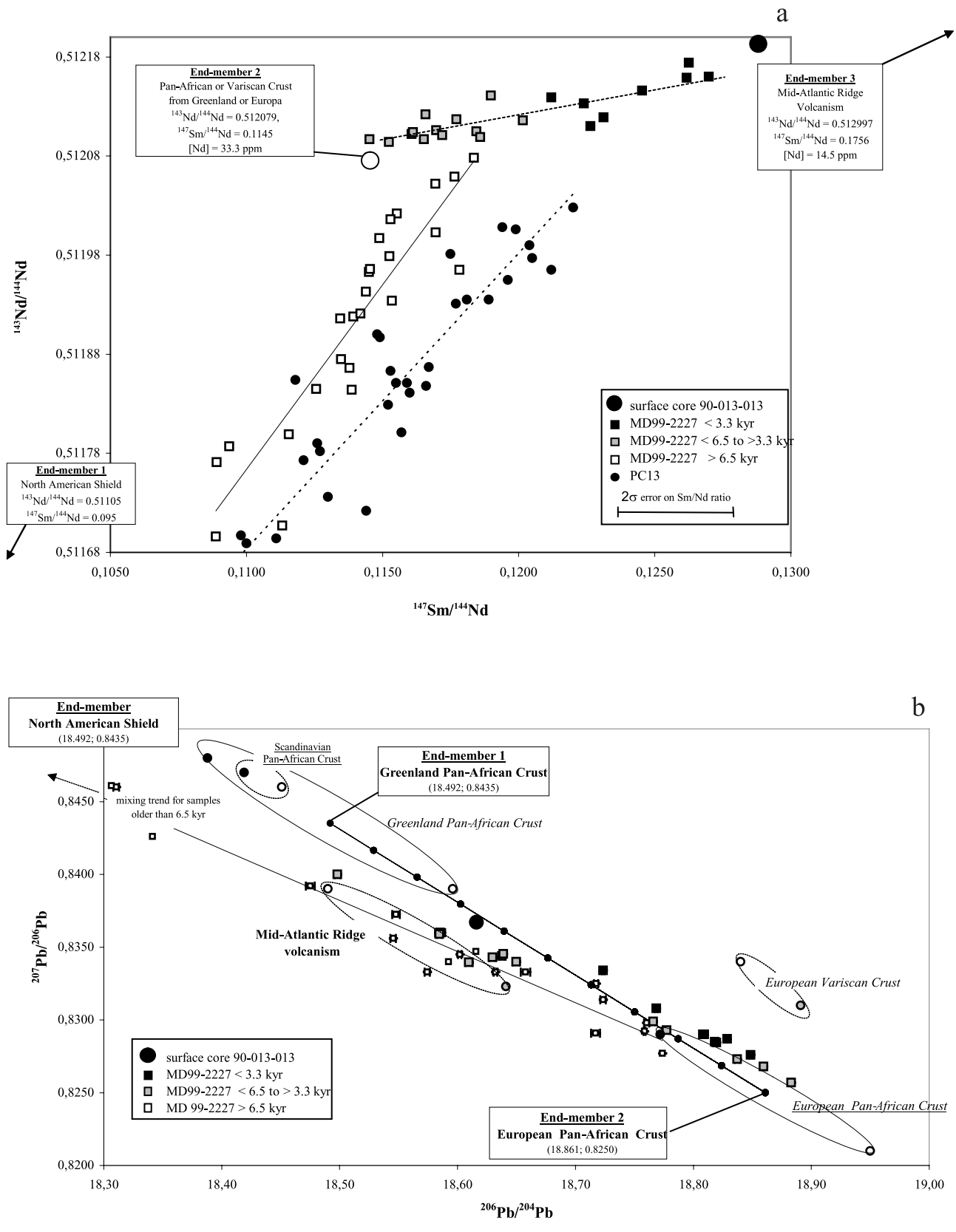
a
End-member 2
Pan-African or Variscan Crust
from Greenland or Europa
143Nd/144Nd = 0.512079,
147Sm/144Nd = 0.1145
[Nd] = 33.3 ppm
End-member 3
Mid-Atlantic Ridge
Volcanism
143Nd/144Nd = 0.512997
147Sm/144Nd = 0.1756
[Nd] = 14.5 ppm
End-member 1
North American Shield
143Nd/144Nd = 0.51105
147Sm/144Nd = 0.095
surface core 90-013-013
MD99-2227 < 3.3 kyr
MD99-2227 < 6.5 to >3.3 kyr
MD99-2227 > 6.5 kyr
PC13
2σ error on Sm/Nd ratio
143Nd/144Nd
147Sm/144Nd
0,51218
0,51208
0,51198
0,51188
0,51178
0,51168
0,1050
0,1100
0,1150
0,1200
0,1250
0,1300
b
End-member
North American Shield
(18.492; 0.8435)
Scandinavian
Pan-African Crust
End-member 1
Greenland Pan-African Crust
(18.492; 0.8435)
mixing trend for samples
older than 6.5 kyr
Greenland Pan-African Crust
Mid-Atlantic Ridge
volcanism
European Variscan Crust
European Pan-African Crust
End-member 2
European Pan-African Crust
(18.861; 0.8250)
surface core 90-013-013
MD99-2227 < 3.3 kyr
MD99-2227 < 6.5 to > 3.3 kyr
MD 99-2227 > 6.5 kyr
207Pb/206Pb
206Pb/204Pb
0,8450
0,8400
0,8350
0,8300
0,8250
0,8200
18,30
18,40
18,50
18,60
18,70
18,80
18,90
19,00

Figure 6

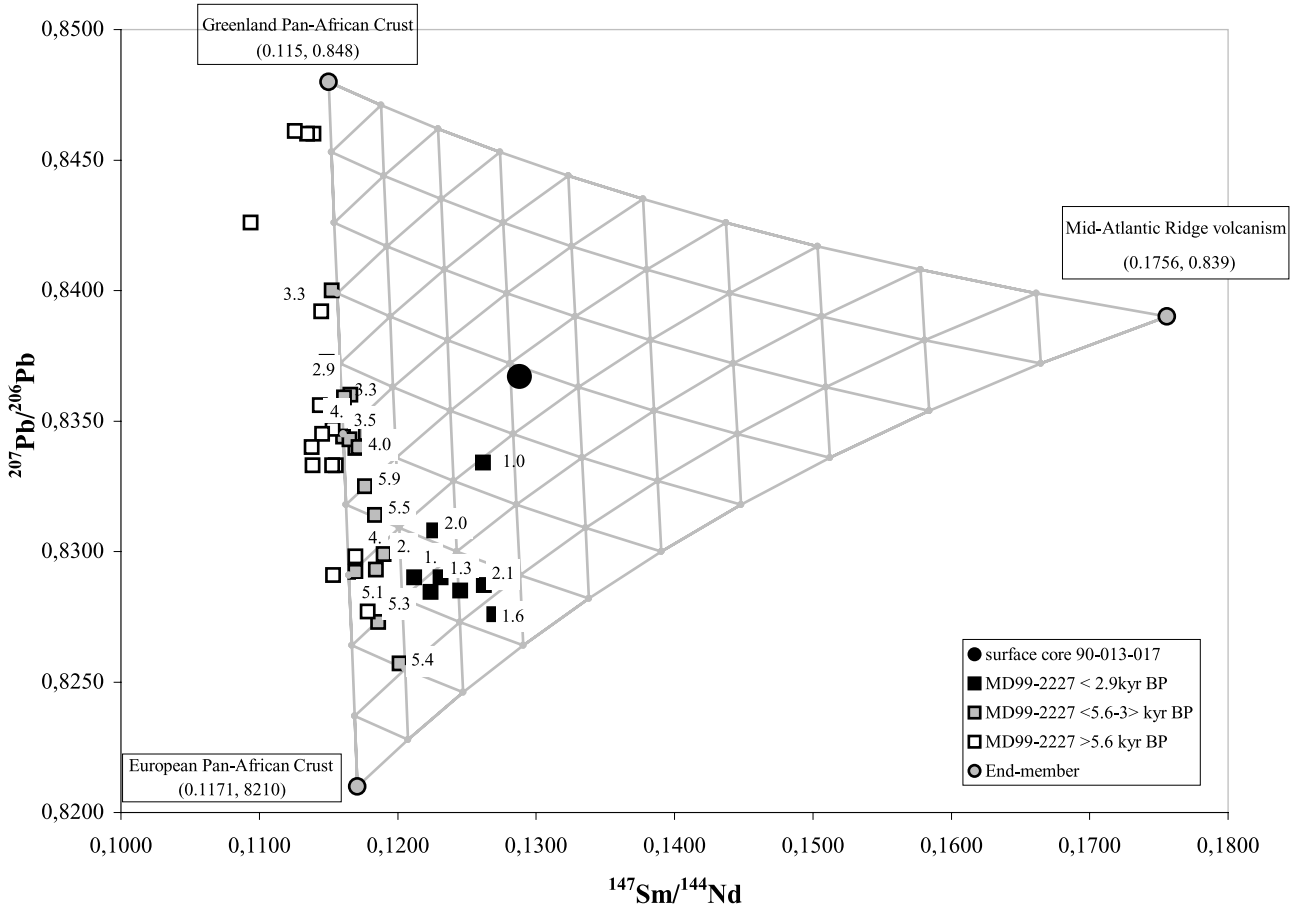

Figure 7. $^{147}Sm/^{144}Nd$ versus $^{207}Pb/^{206}Pb$ diagram. The mixing between the three chosen end-members (i.e., EPC, GPC, and MAR) defines a curved triangle. The grid is calculated according to a 10% increment of the mixture composition. Only the samples younger than 6.5 ka BP fall within the Sm-Pb mixing triangle since the contribution of NAS must be taken into account for older samples. Note the pronounced increase in the MAR contribution in the recent (i.e., <3.3 kyr BP) samples from core MD99-2227 as well as for the representative surface value (from core HU90-013-017).

signatures (Figure 4) and by fluctuations of the mean grain size of the <63 μm fraction (Figure 3). The sedimentary mixtures delivered to the Greenland Rise are predominantly proximal supplies from the Canadian and Greenland margins of the Labrador Sea. In particular, the peak contributions of the NAS end-member at 10 and 8.2 ka might be explained by pulses in the retreat of the corresponding ice sheets inland [*Funder*, 1989; *Barber et al.*, 1999]: (1) In MD99-2227 the 10 ka peak is matched by a decrease of the calcite content within the sediment and by a sharp increase in the mean grain size up to the maximum core value (Figure 3). In PC13 a sharp increase of proximal supplies was also present in the Nd isotope signature at 10.1 ka [*Fagel et al.*, 1999] and can be correlated with mineralogical changes [*Fagel et al.*, 1997]

Figure 6. (a) Enlarged plot of the Nd isotopic signatures of the clay-size fraction (squares). The labels indicate the calibrated age (in kyr BP) of each sample. The linear regression trends (dashed lines) are calculated for two groups of samples, i.e., older than 6.5 kyr (open squares) and younger than 6.5 kyr (filled squares). For the youngest samples, the shaded squares characterize the samples between 6.5 and 3.3 ka, and the black squares the samples <3.3 kyr. The $^{147}Sm/^{144}Nd$ and $^{143}Nd/^{144}Nd$ compositions of NAS are defined in the work of *Innocent et al.* [1997]. The Sm-Nd composition of MAR corresponds to a calculated median value from 52 published data points (see *Fagel et al.* [1999] for statistics). Finally, for the YC we used the representative signature of the Variscan crust as defined in the work of *Fagel et al.* [1999]. (b) Enlarged plot of the MD99-2227 Pb-Pb data subdivided into three same groups as for Figure 6a. The arrow indicates the regression trend defined by the samples older than 6.5 ka. For the samples younger than 6.5 ka, a calculated mixing line between the Greenland and European Pan-African crusts is used. For mixing, we take into account the median value for Greenland Pan-African Crust (GPC) and the mean value for the European Pan-African Crust (EPC).

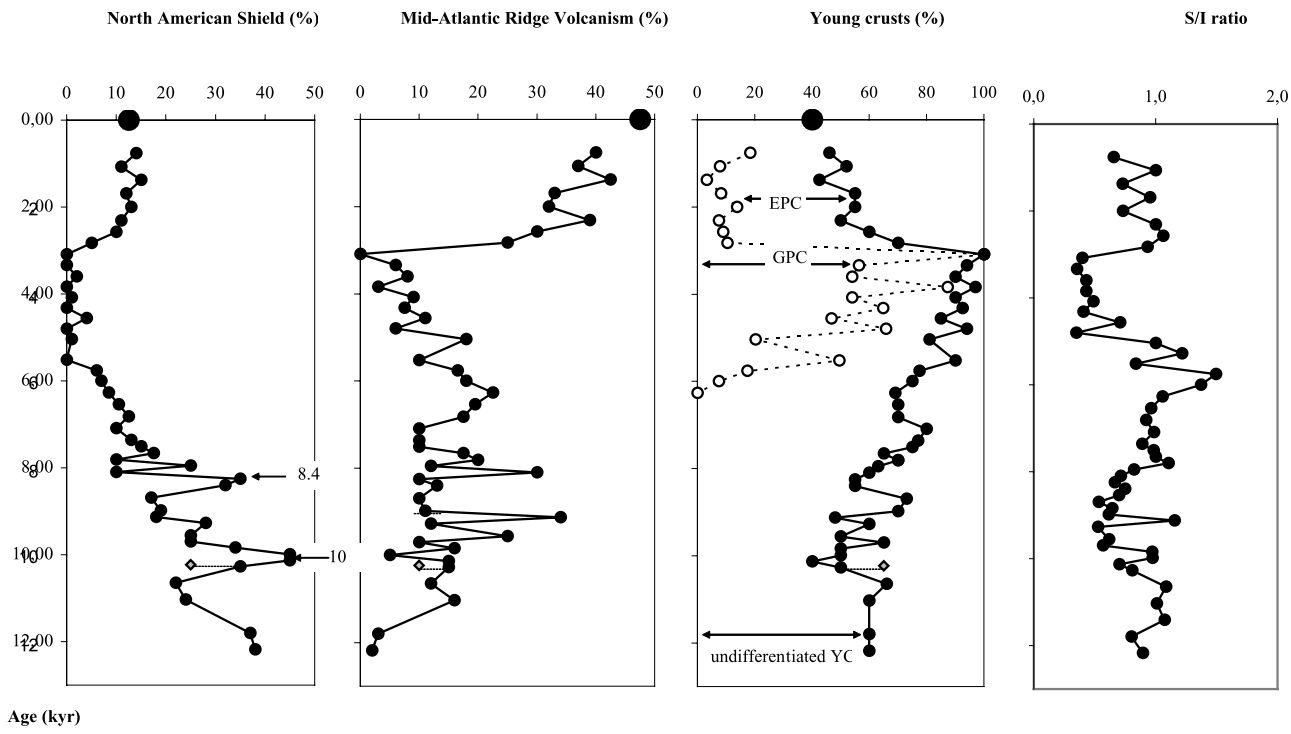

Figure 8. Estimated relative contribution of sediment supplies from the North American Shield, Mid-Atlantic volcanism, and from young crusts over the last 12.2 kyr. See text for explanations. During the last 6.5 kyr, distinct contributions of the Greenland Pan-African crust and from European Pan-African crust can be identified. The surface contribution is plotted as a large circle. The accuracy of the estimation is given by the range of variation obtained from one duplicate (diamond) (i.e., ±10%). The smectite/illite ratio is also reported (see text for explanation).

that have been attributed to a major phase of ice retreat over continental Greenland [*Funder*, 1989]. (2) In MD99-2227 the changes in the Nd and Pb isotopic signatures at 8.2 ka are slightly younger than the large changes in the grain-size parameters of the <63 μm fraction observed at 8.2–8.4 ka (i.e., high mean value, lowest sediment sorting; Table 1). Within the chronological uncertainties that result from the interpolated ages of the present study, the most probable paleoceanographic event that could explain the observed changes is the 8.2 ka major drainage event, when glacial lake Ojibway drained through Hudson Strait [*Barber et al.*, 1999; *Clarke et al.*, 2003]. The grain-size shift in MD-2227 could possibly mark the catastrophic drainage event, whereas the shift in Nd and Pb isotopic compositions record higher proximal NAS-rich supplies. Worth mentioning is the fact that X. W. Meng et al. (Sm-Nd isotopic changes in sediments from the upper continental slope off southeastern Canada, submitted to *Marine Geology*, 2004) observe at this same time interval a large shift in the Nd-isotope composition of sediments cored off Cabot Strait, i.e., at the outlet of the St. Lawrence meltwater route, that they attribute to the rerouting of meltwater of the residual Laurentide Ice Sheet from there to the Hudson Strait area (see also *St-Onge et al.* [2003] for the dating of the accompanying sedimentary rerouting event).

6.1.2.2. Time Period 7.7 to 5.8 ka

[27] The NAS contribution decreases gradually toward zero during this interval and is counterbalanced mainly by an increase in young crustal material, mostly EPC. Within this time slice the S/I ratio reached its maximum value of 1.5 at 5.8 ka (Figure 8 and Table 1). Within the clays the increase in smectite abundance (up to 36%; Table 1) probably reflects a larger contribution of distal supplies. This interval is also characterized by a change in the ratio between the detrital and biogenic fractions of the sediment. For instance, the contribution of biogenic calcite (within the <106 μm fraction) increases from 10 to 40% between 8.4 and 7.7 ka. The sedimentation rate also drops by a factor of 2 within this interval, decreasing from ~70 cm/kyr before 7.4 ka to 37 cm/kyr after 7.4 ka. These sedimentological changes agree with the timing of the final melting stage of the Laurentide Ice Sheet, thus marking the vanishing meltwater supply from the Quebec-Labrador peninsula into the Labrador Sea [*Licciardi et al.*, 1999; *Jansson*, 2003]. The subsequent increase in biogenic productivity marks the Holocene climate optimum in the sub-Arctic seas [e.g., *Andrews et al.*, 2003; *Solignac et al.*, 2004]. The period around 6.5 kyr BP is indeed generally described as the peak warm period in the North Atlantic Ocean and Norwegian-Greenland Sea records [e.g., *Rasmussen et al.*, 2002]. For instance, in core DS97-4P from the southeast Greenland margin, the maximum carbonate content is recorded at a ^{14}C age of 5.38 kyr (i.e., 6 kyr in calendar age; *Kuijpers et al.* [2003]).

6.1.2.3. Time Period 5.5 to 3.3 ka

[28] The NAS contribution remains close to 0, whereas the GPC contribution increases sharply, up to 90% at the end of this interval. There is no related change in the core

mineralogy, nor does the biogenic/detrital sediment ratio change. Within clays the smectite abundances and the S/I ratios decrease to their lowest values at the end of this interval (i.e., 18% and 0.35). The evolution of the S/I ratio illustrates the relative contribution of Mid-Atlantic Ridge volcanism. The isotopic and mineralogical changes observed in the clay fraction thus agree with a change in the source of distal supplies, with a proximal NAS contribution being close to 0.

6.1.2.4. Time Period 3.1 ka to Present

[29] The MAR contribution increases significantly, from 10 to 40%, and the young crust material is derived primarily from European Pan-African crust. The increase in the S/I ratio most probably reflects a relative change in the current-driven clay assemblage rather than an enhanced smectite flux (Figure 8). The overall clay supply remains quite constant, as indicated by the absence of change in sedimentation rate from the previous time slice and the lack of change in the biogenic/detrital ratio). The observed change in sedimentary mixtures is also associated with a marked decrease in the mean grain size. This suggests that the hydrodynamic regime could have been less active, in agreement with the late Holocene decrease reported in the sandy fraction of southeast Greenland margin sediments [*Kuijpers et al.*, 2003].

6.2. Paleoceanographic Implications

[30] The clay-size material delivered to the MD99-2227 site is mainly carried by the WBUC that drives the present DSOW and NEADW into the Labrador Sea (Figure 1). Our interpretation of paleoceanographic changes is based on the following:

[31] 1. There are two main current pathways that transport sediment particles through the Iceland and Irminger basins toward the Labrador Sea.

[32] 2. The western current pathway can be identified by its Pan-African Nd and Pb isotope signature from east Greenland, carried by the present DSOW water mass. The eastern pathway is characterized by its Pan-African Nd and Pb isotope signature from northwestern Europe and is carried to the Labrador Sea by the modern NEADW.

6.2.1. Isotopic Fingerprint of the Particles Driven by DSOW and NEADW

[33] The isotopic fingerprint of the particles carried by the DSOW is characterized by its Pan-African Nd signature. Owing to its geographical location, DSOW is the principal water mass capable of supplying particles eroded from the east Greenland margin. This assumption is in agreement with Sm-Nd isotope signatures of northeastern North Atlantic surface sediments: the presence of Pan-African Nd has only been reported in sites bathed by the DSOW in the Irminger Basin [*Innocent et al.*, 1997].

[34] The Pan-African Nd signature of DSOW is mainly attributed to the Paleozoic sedimentary rocks of northeastern Greenland (Figure 1), but we cannot rule out some contribution of SPC in the DSOW fingerprint for two reasons. First, particles from the Scandinavian margin could be carried to the Denmark Strait through the Nordic Seas cyclonic gyres (Figure 1). Second, SPC has an isotope signature close to that of the GPC (e.g., Figures 5a and 6b). The exact origin of DSOW, and in particular its contribution from Iceland Basin, remains unclear [*Lacan and Jeandel*, 2004]. Whatever the origin, the DSOW water mass transports particles having a Pan-African Nd signature from both the GPC and SPC to the WBUC through the same (western) pathway.

[35] Because of the morphology of the eastern basins, the eastern pathway is longer and its Phanerozoic European-derived isotope signature is diluted by volcanic inputs from Iceland and the Reykjanes ridge. In the Iceland Basin the Nd signature of surface sediments bathed by NEADW has been interpreted as a simple mixture between two end-members, i.e., the MAR volcanism and a component having a Sm-Nd signature of Variscan crust [*Innocent et al.*, 1997].

6.2.2. Evolution of Deep Currents Inferred From Isotopic Signatures of the Clay Fraction

[36] In core PC13, there is no evidence of DSOW overflow until at least 8.6 ka. In view of the geographic position of the end-members (see Figure 1), the significant increase in GPC between 6.5 and 3 ka in MD99-2227 could reflect relatively higher supplies from the DSOW. Recently, *Kuijpers et al.* [2003] have observed a coarsening upward trend within the fine sand fraction that dominates the middle to late Holocene surface sediments of core DS97-7P (southeast Greenland, 1843 m water depth). They attributed this sedimentological change to an increase in velocity of the DSOW current, leading to enhanced water mass exchange between the Greenland Sea and the Irminger Basin. *Kuijpers et al.* [2003] suggested that the maximum DSOW flow intensity may have been linked to the shift of the Polar Front to its present-day position. Within the clay-size supplies, the changes in the relative contribution of the two Phanerozoic crusts (i.e., GPC and EPC) through the middle and late Holocene suggest a change in the main sediment transport pathways. Within a simple two end-member sediment mixing model, we therefore interpret the evolution of the GPC/EPC ratio by a change in the DSOW component of the WBUC relative to the NEADW component.

[37] South of 60°S in the east Atlantic, *Sarnthein et al.* [1994] demonstrated that the Holocene mode of deep water circulation, monitored by cores in the depth range of the NADW, was fully established by about 9.1–9.5 ^{14}C kyr ago (i.e., after 10.5 ka in calendar age). However, our Nd and Pb isotope data from the Labrabor Sea clay-size fraction suggest that the relative contributions of the main components of the NADW changed during the Holocene. The main oceanographic feature is a pulse in the DSOW contribution after the mid-Holocene (i.e., between 6.5 and 3 ka) that may be related to the inception of the DSOW. However, such an assumption still needs to be confirmed by additional isotope studies on other grain-size fractions. By working on the clay-size fraction, we get a biased, or at least only partial, view of the system. The DSOW signal has been imprinted on the isotopic signature of the clay-size fraction since 6.5 ka, but this does not necessarily mean that DSOW was absent before 6.5 ka. However, after 3 ka the contribution of DSOW decreased, reaching the present surface compositions (young crust composed of 65% GPC and 35% EPC) by 2 ka. Another element worthy of mention here

concerns the effects that the inception of convection in the Labrador Sea, with formation of the near 2000 m deep Labrador Seawater mass overlying NADW, would have had on the emplacement and dynamic properties of the WBUC that carried these water masses into the deep Labrador Sea. On the basis of various arguments, *Hillaire-Marcel et al.* [2001a, 2001b] and *Solignac et al.* [2004] conclude that LSW formation has been enhanced during the late Holocene (with respect notably to DSOW). The recent increase in NAS (Figure 8) could record some greater influence of LSW that could drive proximal supplies from Labrador Sea margins.

7. Conclusion and Perspectives

[38] The Nd and Pb isotope signatures of the clay-size fraction from core MD99-2227 off south Greenland were used to reconstruct sedimentary provenance and paleocirculation within the Labrador Sea through the Holocene. Before 8.4 ka, current-induced changes in sediment composition are masked by the signature of large proximal sediment supplies. Major punctuated discharges at 10 and 8.2 ka could be related to the retreat of the ice sheet over continental Greenland and the final drainage of large glacial lakes in eastern Canada. Between 8.4 and 6.5 ka, the distal current delivered supplies increase with the establishment of full deglacial conditions in the Labrador Sea. The modern deepwater circulation pattern was not yet established. From 6.5 to 3 ka the appearance of major supplies of material from Greenland Pan-African crust is attributed to the strong influence of the DSOW. The change in sediment provenance probably corresponds to inception of the DSOW, but further isotope investigations on the silt fractions must be done in order to confirm this hypothesis. After 3 ka the modern deep circulation pattern, with enhanced influence of LSW formation, was gradually established. In contrast to evidence for stable Holocene deepwater ventilation of the southern Atlantic Ocean, our Nd and Pb isotope records implicate significant changes in the relative contribution of the principal present-day NADW components.

[39] **Acknowledgments.** We thank NSERC-CANADA and the IMAGES program for access to cores. This work was made easier with the help of Helene Isnard, Maryse Henry, Jean-François Larrivière, and Michel Preda from the GEOTOP at UQAM, Claude Maerschalk and Jeroen de Jong at ULB, and Sébastien Betrand from ULg. Onshore studies were supported by several research organizations, notably FNRS and the Faculty of Sciences at ULg in Belgium and NSERC and the UNESCO Chair for Global Change Study in Canada. Discussions with C. Innocent (BRGM, France) and N. Mattielli (ULB) were particularly helpful in improving the manuscript. This manuscript corresponds to the publication MARE040. This work is dedicated to the memory of Clement Gariépy from the GEOTOP.

References

Andrews, J. T., J. Hardadottir, J. S. Stoner, M. E. Mann, G. B. Kristjansdottir, and N. Koc (2003), Decadal- to millennial-scale periodicities in north Iceland shelf sediments over the last 12,000 cal yr: Long-term North Atlantic oceanographic variability and solar forcing, *Earth Planet. Sci. Lett.*, *210*, 453–465.

Barber, D. C., et al. (1999), Forcing the cold event of 8200 years ago by catastrophic drainage of Laurentide lakes, *Nature*, *400*, 344–348.

Bilodeau, G., A. de Vernal, and C. Hillaire-Marcel (1994), Benthic foraminiferal assemblages in Labrador Sea sediments: Relations with deep-water mass changes since the deglaciation, *Can. J. Earth Sci.*, *31*, 128–138.

Biscaye, P. E. (1965), Mineralogy and sedimentation of recent deep-sea clay in the Atlantic and adjacent seas and oceans, *Geol. Soc. Am. Bull.*, *76*, 803–832.

Boski, T., J. Pessoa, P. Pedro, J. Thorez, J. M. A. Dias, and I. R. Hall (1998), Factors governing abundance of hydrolysable amino acids in the sediments from the NW European continental margin (47–50°N), *Prog. Oceanogr.*, *42*, 145–164.

Boyle, E. A. (1995), Last Glacial Maximum North Atlantic Deep Water: On, off or somewhere in between? Philos, *Trans. R. Soc. London Ser. A*, *348*, 243–253.

Brasseur, R. (2002), Evolution de la signature isotopique en Pb des sédiments de la Mer du labrador au cours de l'Holocène: Implications sur la circulation océanique profonde en Atlantique Nord, *Mem. DEA, Oceanogr.*, 66 pp., Univ. of Liège, Liège.

Bridgewater, D., M. Marker, and F. Mengel (1991), The eastern extension of the early Proterozoic orogenic zone across the Atlantic, *Rep. ECSOOT Transect Meet.*, *34*, 100–107.

Broecker, W. S., and G. H. Denton (1989), The role of ocean-atmosphere reorganisation in glacial cycle, *Geochim. Cosmochim. Acta*, *53*, 63–89.

Campbell, L. M., D. Bridgewater, and G. L. Farmer (1996), A comparison of Proterozoic crustal formation along the Torngat-Nagssugqtoqidian-Lapland collision belts: Preliminary constraints from Nd and Pb isotopic studies in northern Labrador, *Rep. ECSOOT Transect Meet.*, *45*, 22–36.

Clarke, G., D. Leverington, J. Teller, and A. Dyke (2003), Enhanced: Superlakes, megafloods and abrupt climate change, *Science*, *301*, 922–923.

de Vernal, A., C. Hillaire-Marcel, J. L. Thuron, and J. Matthiessen (2000), Reconstruction of sea surface temperature, salinity, and sea ice cover in the northern North Atlantic during the Last Glacial Maximum based on dinocyst assemblages, *Can. J. Earth Sci.*, *37*, 725–750.

Dia, A., B. Dupré, and C. J. Allègre (1992), Nd isotopes in Indian Ocean used as a tracer of supply to the ocean and circulation paths, *Mar. Geol.*, *103*, 349–359.

Dickson, R. R., and J. Brown (1994), The production of North Atlantic Deep Water: Sources, rates, and pathways, *J. Geophys. Res.*, *99*, 12,319–12,341.

Duplessy, J.-C., E. Ivanova, I. Murdmaa, M. Paterne, and L. Labeyrie (2001), Holocene paleoceanography of the northern Barents Sea and variations in the northward heat transport of the Atlantic Ocean, *Boreas*, *30*, 2–16.

Fagel, N., C. Hillaire-Marcel, and C. Robert (1997), Changes in the Western Boundary Undercurrent outflow since the Last Glacial Maximum, from smectite/illite ratios in deep Labrador Sea sediments, *Paleoceanography*, *12*, 79–96.

Fagel, N., C. Innocent, R. K. Stevenson, and C. Hillaire-Marcel (1999), Deep circulation changes in the Labrador Sea since the Last Glacial Maximum: New constraints from Sm-Nd data on sediments, *Paleoceanography*, *14*, 777–788.

Fagel, N., C. Innocent, C. Gariépy, and C. Hillaire-Marcel (2002), Sources of Labrador Sea sediments since the Last Glacial Maximum inferred from Nd-Pb isotopes, *Geochim. Cosmochim. Acta*, *66*, 2569–2581.

Fagel, N., T. Boski, L. Likhoshway, and H. Oberhaensli (2003), Late Quaternary clay mineral record in Central Lake Baikal (Academician Ridge Siberia), *Palaeogeogr. Palaeoecol. Palaeoecol.*, *193*, 159–179.

Faure, G. (1986), *Principles of Isotope Geology*, 589 pp., John Wiley, Hoboken, N. J.

Folk, R. L., and W. C. Ward (1957), Brazos River bar: A study in the significance of grain-size parameters, *J. Sediment. Petrol.*, *27*, 3–26.

Frank, M. (2002), Radiogenic isotopes: Tracers of past ocean circulation and erosional input, *Rev. Geophys.*, *40*(1), 1001, doi:10.1029/2000RG000094.

Funder, S. (1989), Quaternary geology of the ice-free areas and adjacent shelves of Greenland, in *Quaternary Geology of Canada and Greenland*, *Geology of Canada.* edited by R. J. Fulton, pp. 743–792, Geol. Surv. of Can., Ottawa, Ont.

Galer, S. J. G. (1999), Optimal double and triple spiking for high precision lead isotopic measurement, *Chem. Geol.*, *154*, 255–274.

Hansen, B., and S. Osterhus (2000), North Atlantic-Nordic Seas exchanges, *Prog. Oceanogr.*, *45*, 109–208.

Hillaire-Marcel, C., A. De Vernal, G. Bilodeau, and G. Wu (1994), Isotope stratigraphy, sedimentation rates, deep circulation and carbonate events in the Labrador Sea during the last ~200 ka, *Can. J. Earth Sci.*, *31*, 63–89.

Hillaire-Marcel, C., A. de Vernal, G. Bilodeau, and A. J. Weaver (2001a), Absence of deep water formation in the Labrador Sea during the last interglacial period, *Nature*, *410*, 1073–1077.

Hillaire-Marcel, C., A. de Vernal, G. Bilodeau, and J. Stoner (2001b), Changes of potential density gradients in the northwestern North Atlantic during the last climatic cycle, based on a multi-proxy approach, in *The Oceans and Rapid Climate Change: Past, Present, and Future*, *Geophys. Monogr. Ser.*, vol. 126, edited by D. Seidov et al., pp. 83–100, AGU, Washington, D. C.

Hillaire-Marcel, C., A. de Vernal, L. Polyak, and D. Darby (2004), Size dependent isotopic compositions of planktic foraminifers from the Chukchi Sea vs. NW Atlantic sediments—Implications for the Holocene paleoceanography of the western Arctic, *Quat. Sci. Rev.*, *23*, 245–260.

Humblet, M. (2002), Evolution de la signature isotopique en Nd et Sm des sédiments de la Mer du Labrador au cours de l'Holocène: Implications sur la circulation océanique profonde en Atlantique Nord, *Mem. DEA, Oceanogr.*, 76 pp., Univ. of Liège, Liège.

Innocent, C., N. Fagel, R. K. Stevenson, and C. Hillaire-Marcel (1997), Sm-Nd signature of modern and late Quaternary sediments from the northwest North Atlantic: Implications for deep current changes since the Last Glacial Maximum, *Earth Planet. Sci. Lett.*, *146*, 607–625.

Jansson, K. N. (2003), Early Holocene glacial lakes and ice marginal retreat pattern in Labrador/Ungava, Canada, *Palaeogeogr. Palaeoclimatol. Palaeoecol.*, *193*, 473–501.

Kalsbeek, F., H. Austrheim, D. Bridgewater, B. T. Hansen, S. Pedersen, and P. N. Taylor (1993), Geochronology of Archaean and Proterozoic events in the Ammassalik area, southeast Greenland, and comparisons with the Lewisian of Scotland and the Nagssugtoqidian of west Greenland, *Precambrian Res.*, *62*, 239–270.

Kuijpers, A., S. R. Troestra, M. A. Prins, K. Linthout, A. Akhmetzhanov, S. Bouryak, M. F. Bachmann, S. Lassen, S. Rasmussen, and J. B. Jensen (2003), Late Quaternary sedimentary processes and ocean circulation changes at the southeast Greenland margin, *Mar. Geol.*, *195*, 109–129.

Lacan, F., and C. Jeandel (2004), Denmark Strait Water circulation traced by heterogeneity in neodymium isotopic compositions, *Deep Sea Res.*, *51*, 71–82.

Ledbetter, M. T., and W. M. Balsam (1985), Paleoceanography of the deep western boundary undercurrrent on the North American continental margin for the past 25,000 yr, *Geology*, *13*, 181–184.

Licciardi, J. M., J. T. Teller, and P. U. Clark (1999), Freshwater routing by the Laurentide ice sheet during the last deglaciation, in *Mechanisms of Global Climate Change at Millennial Time Scales*, *Geophys. Monogr. Ser.*, vol. 112, edited by P. U. Clark, R. S. Webb, and L. D. Keigwin, pp. 177–201, AGU, Washington, D. C.

Lucotte, M., and C. Hillaire-Marcel (1994), Identification des masses d'eau dans les mers du Labrador et d'Irminger, *Can. J. Earth Sci.*, *31*, 5–13.

Manhès, G., J. F. Minster, and C. J. Allègre (1978), Comparative uranium-thorium-lead and rubidium-strontium study of the Saint-Séverin amphoterite: Consequences for early solar system chronology, *Earth Planet. Sci. Lett.*, *39*, 14–24.

McCartney, M. S. (1992), Recirculating components to the deep boundary current of the northern North Atlantic, *Prog. Oceanogr.*, *29*, 283–383.

McCave, I. N., B. Manighetti, and N. A. S. Beveridge (1995), Circulation in the glacial North Atlantic inferred from grain-size measurements, *Nature*, *374*, 149–151.

Moore, D. M., and R. C. Reynolds (1989), *X-Ray Diffraction and the Identification and Analysis of Clay Minerals*, 332 pp., Oxford Univ. Press, New York.

Rasmussen, T. L., D. Bâckstrôm, J. Heinemeier, D. Klitgaard-Kristensen, P. C. Knutz, A. Kuijpers, S. Lassen, E. Thomsen, S. R. Troelstra, and T. C. E. van Weering (2002), The Faroe-Shetland gateway: Late Quaternary water mass exchange between the Nordic seas and the northeastern Atlantic, *Mar. Geol.*, *188*, 165–192.

Revell, M., M. Cremer, F. E. Grousset, and L. Labeyrie (1996), Grain-size and Sr-Nd isotopes as tracer of paleo-bottom current strength, northeast Atlantic Ocean, *Mar. Geol.*, *131*, 233–249.

Rosman, K. J. R., and P. D. P. Taylor (1998), Isotopic compositions of the elements 1997, *Pure Appl. Chem.*, *70*, 217–236.

Sarnthein, M., K. Winn, S. Jung, J. Duplessy, L. Labeyrie, H. Erlenkeuser, and G. Ganssen (1994), Changes in east Atlantic deepwater circulation over the last 30,000 years: Eight time slice reconstructions, *Paleoceanography*, *9*(2), 209–268.

Schmitz, W. J., and M. S. McCartney (1993), On the North Atlantic circulation, *Rev. Geophys.*, *31*, 29–49.

Solignac, S., A. de Vernal, and C. Hillaire-Marcel (2004), Holocene sea-surface conditions in the North Atlantic—Contrasted trends and regimes between the eastern and western sectors (Labrador Sea vs. Iceland Basin), *Quat. Sci. Rev.*, *23*, 319–334.

St-Onge, G., J. S. Stoner, and C. Hillaire-Marcel (2003), Holocene paleomagnetic records from the St. Lawrence Estuary, eastern Canada: Centennial- to millennial-scale geomagnetic modulation of cosmogenic isotopes, *Earth Planet. Sci. Lett.*, *209*, 113–130.

Stuiver, M., and P. J. Reimer (1993), Extended ^{14}C data base and revised CALIB3.0 14C age calibration program, *Radiocarbon*, *35*, 215–230.

Turon, J. L., et al. (1999), Images V, à bord du "Marion Dufresne", 2^{e} Leg du 30 juin au 24 juillet 1999, *Rapp. Mission 99-X*, Inst. Fr. de Rech. en Terres Polaires, Brest.

Veiga-Pires, C. C., and C. Hillaire-Marcel (1998), U and Th isotope constraints on the duration of Heinrich events H0–H4 in the southern Labrador Sea, *Paleoceanography*, *14*, 187–199.

von Blanckenburg, F., and T. F. Nägler (2001), Weathering versus circulation-controlled changes in radiogenic isotope tracer composition of the Labrador Sea and North Atlantic Deep Water, *Paleoceanography*, *16*, 424–434.

Wasserburg, G. J., S. B. Jacobsen, D. J. De Paolo, M. T. McCulloch, and T. Wen (1981), Precise determination of Sm/Nd ratios, Sm and Nd isotopic abundances in standard solutions, *Geochim. Cosmochim. Acta*, *45*, 2311–2323.

White, W. M., F. Albarède, and P. Télouk (2000), High-precision analysis of Pb isotopic ratios using multi-collector ICP-MS, *Chem. Geol.*, *167*, 257–270.

R. Brasseur, N. Fagel, and M. Humblet, UR Clay and Paleoclimate and Mare, Department of Geology and Oceanography, University of Liège, B18, Allée du 6 Août, B-4000 Liège, Belgium. (nathalie.fagel@ulg.ac.be)

C. Hillaire-Marcel and R. Stevenson, Centre de Recherches en Géochimie et Géodynamique (GEOTOP), Université du Québec à Montréal, CP 8888, Montréal, Québec H3C 3P8, Canada.

D. Weis, Pacific Center for Isotopic and Geochemical Research, University of British Columbia, 6339 Stores Road, Vancouver V6T 1Z4, B. C., Canada.